Electronic transport in disordered n -alkanes: From fluid methane to amorphous polyethylene

David Cubero, Nicholas Quirke, and David F. Coker

Citation: The Journal of Chemical Physics **119**, 2669 (2003); doi: 10.1063/1.1587130
View online: http://dx.doi.org/10.1063/1.1587130
View Table of Contents: http://scitation.aip.org/content/aip/journal/jcp/119/5?ver=pdfcov
Published by the AIP Publishing

Electronic transport in disordered *n*-alkanes: From fluid methane to amorphous polyethylene

David Cubero and Nicholas Quirke[a)]
Department of Chemistry, Imperial College, London, SW7 2AY, United Kingdom

David F. Coker
Department of Chemistry, Boston University, Boston, Massachusetts 02215

(Received 28 February 2003; accepted 7 May 2003)

We use a fast Fourier transform block Lanczos diagonalization algorithm to study the electronic states of excess electrons in fluid alkanes (methane, ethane, and propane) and in a molecular model of amorphous polyethylene (PE) relevant to studies of space charge in insulating polymers. We obtain a new pseudopotential for electron–PE interactions by fitting to the electronic properties of fluid alkanes and use this to obtain new results for electron transport in amorphous PE. From our simulations, while the electronic states in fluid methane are extended throughout the whole sample, in amorphous PE there is a transition between localized and delocalized states slightly above the vacuum level ($\sim +0.06$ eV). The localized states in our amorphous PE model extend to -0.33 eV below this level. Using the Kubo–Greenwood equation we compute the zero-field electron mobility in pure amorphous PE to be $\mu \approx 2 \times 10^{-3}$ cm^2/V s. Our results highlight the importance of electron transport through extended states in *amorphous* regions to an understanding of electron transport in PE. © *2003 American Institute of Physics.* [DOI: 10.1063/1.1587130]

I. INTRODUCTION

Polyethylene is commonly used as an insulator for high-voltage electric cables.[1] A long standing problem with polymeric insulators is that they trap charge, to form what is usually described as a ''space charge.'' There is a vast literature concerned with the experimental characterization of space charge (methods[2] include thermal step,[3] pulsed electroacoustic,[4] thermal pulse,[5] pressure pulse,[6] photoconductivity,[7] and mirror image[8]). It is believed that electrical breakdown in dielectric polymers is closely related to the creation of space charge in the material[9] linked to both its chemical and physical characteristics. Thus, a model to predict the lifetime of the insulating material would naturally include a description of the space charge and its relation to the chemical and physical microstructure. Several phenomenological models have been developed to explain the formation[10] as well as the role of the space charge in electrical aging.[11] Nevertheless, a clear identification of its molecular origin is not yet available. An understanding of space charge accumulation and its link to dielectric breakdown would be a major scientific achievement as well as facilitating the prediction of cable lifetimes and the design of better cables.

In our previous work we have identified physical and chemical traps in model alkane waxes thought to approximate the local structure of amorphous polyethylene and characterized them using *ab initio* methods.[12,13] This information has been used to predict the current voltage characteristics of model polyethylene with some success.[14] However the earlier calculations of electron trapping were limited to the effects of conformational defects with respect to the ground state of the all-*trans* long chain alkane molecule and were not capable of capturing information on the role of local density changes associated with local disorder in amorphous polyethylene (PE) or the details of excess electron states in more complete representations of crystalline polyethylene. In addition all previous calculations were for ground states. In the present paper we use a fast Fourier transform block Lanczos diagonalization algorithm to study the electronic states and mobility of excess electrons in amorphous polyethylene (PE), developing a new pseudopotential for electron–PE interactions by fitting to the electronic properties of fluid alkanes.

The behavior of excess electrons in *n*-alkane fluids has been extensively investigated[15–19] and represents a paradigm for the study of the transport properties of excess electrons in dielectric media. There are numerous measurements of the low-field electron mobility μ and the conduction band energy V_0, defined as the difference of the photoelectric work function of a metal electrode when in contact with the material and in vacuum. These two quantities are usually correlated,[20] indeed for spherical molecules such as methane or neopentane the maximum in μ appears at about the same density as the minimum in V_0. This correspondence can be explained in terms of a deformation potential theory[21] assuming that the electronic states are extended. In chain molecules such as *n*-alkanes the mobility can decrease by several orders of magnitude as the fluid density varies; this has been attributed to localized states trapping electrons.[22]

In what follows we report results for the electronic states and zero-field mobilities of excess electrons in alkane fluids and in amorphous PE using a pseudopotential technique. The new data for amorphous PE allow us to clarify earlier dis-

a)Electronic mail: n.quirke@imperial.ac.uk

cussions of space charge and its relation to electron trapping by physical defects.[9] We have reported some preliminary results for the electronic states in polyethylene and alkane crystals elsewhere.[23,24] Note that in what follows we report electronic states corresponding to configurations taken from classical molecular dynamics simulation *unperturbed by the presence of the excess electron*. This does not affect the main results reported in this paper or our previous paper,[25] since we are mainly concerned in conduction through extended states, where the electron propagates fast enough that we can neglect any perturbation of the slow molecular trajectories by the electron.

The order of magnitude of the electron mobility is determined by the nature of the electronic wave functions (i.e., extended versus localized). Indeed in the modern theory of the insulating state,[26] an insulator is characterized by the localization of the many-body ground state wave function. There are a number of possible criteria for localization of a single electron wave function available in the literature.[27–29] However, most of them involve studying the behavior of the eigenstates as the system becomes larger, and thus are difficult to apply in the context of periodic systems when there are computational limitations on the system size. Edwards and Thouless have proposed a method based on the sensitivity of the energy levels to the boundary conditions.[28,30] When changed from periodic to antiperiodic boundary conditions, the energy levels should be shifted. If the eigenstates are extended the shift varies as L^{-2}, where L is the length of the system, but if localized as D the electron diffusion constant, and the energy shift is exponentially small. However, this method is not easy to implement in the version of the Lanczos diagonalization method[31] that we wish to use for this study. As a result we have developed a new criterion for localization that does not involve changes in the system length or the boundary conditions. With our approach, calculations on different size systems still need to be performed to decide if the properties of the small periodic systems we can study are representative of the bulk systems in which we are interested. Our strategy is to test pseudopotentials and localization methods on the fluid alkanes and then apply this approach to the problem of the electronic structure and electron mobilities in amorphous polyethylene

The paper is organized as follows: In Sec. II we describe the localization criterion method, the Kubo–Greenwood equation we have used to compute electronic mobilities, and the simulation details. In Sec. III we describe the electron–alkane pseudopotential. The results of the simulations and calculations are presented in Sec. IV. Finally, Sec. V provides a short summary and conclusions.

II. METHODOLOGY

A. Localization criterion

Assume we have computed the eigenstates $\psi_E(\mathbf{r})$ of the one-electron Hamiltonian H in a box of side L For simplicity, we will consider Born–von Karman boundary conditions at $x=\pm L/2$. Starting from the operator formula $[x,H]=i\hbar p_x/m$ we have

$$i\langle \psi_{E'}|p_x|\psi_E\rangle = \frac{m(E-E')}{\hbar}\langle \psi_{E'}|x|\psi_E\rangle + \Phi_x(L/2), \quad (1)$$

where Φ_x is a flux contribution involving a surface integral at the boundary of the box

$$\Phi_x(x_B) = \frac{\hbar}{2}\int_{x=x_B} dy\, dz \left(\psi^*_{E'}\frac{\partial}{\partial x}\psi_E - \psi_E \frac{\partial}{\partial x}\psi^*_{E'} \right). \quad (2)$$

Equation (1) is usually presented without the boundary contribution Φ_x, because it is assumed that the wave function goes to zero when the boundaries are taken to infinity, but this only applies for the special case of localized states. From Eq. (1) it is clear that localized eigenstates can only have vanishing expected momenta (when $E'=E$), they do not propagate. For extended states the flux contribution is very important, becoming dominant when the two states correspond to energies that are very close. This can be used as a sign of delocalization: when the flux Φ_x is comparable to the first term in Eq. (1) the states are extended. However, there is a technical difficulty which comes from the fact that the position operator x and thus $\langle \psi_{E'}|x|\psi_E\rangle$, is not well defined under periodic boundary conditions (nor with extended states). Its matrix elements, as well as Φ_x, depend on the particular choice for the position of the origin of the system x_0 (chosen at any point inside the unit cell), which in turn determine the boundaries at $x_B=x_0\pm L/2$. This is not a real problem for extended states, because the boundary contribution becomes dominant and thus independent of the boundary position [the left-hand side of Eq. (1) is boundary position independent], but can lead to errors for localized states if the system size is small compared to the localization length as discussed in the following.

Assume that $\psi_E(\mathbf{r})$ is localized around some point in the unit cell. Because of the boundary conditions, it will be localized around all equivalent points in the periodic images of the unit cell. If we place the boundaries in a region where the wave function $\psi_E(\mathbf{r})$ is small, the contribution Φ_x will be exponentially small, indicating localization. But if the boundary is in the middle of the localized wave function, Φ_x will provide an appreciable contribution, which might be wrongly interpreted as a sign of delocalization. Therefore, we propose to compute Φ_x as a function of the boundary position x_B, and take the value that corresponds to the minimum in absolute value. If the minimum absolute value of the boundary term is comparable with $\langle \psi_{E'}|x|\psi_E\rangle$ or equivalently with the momentum matrix element, the states are delocalized. However, if this boundary term is much smaller than the volume term, the states are localized provided our model system is large enough to contain the localized wave function. These procedures can be applied to the other spatial components, providing a reliable criterion for localization.

We recall that because of time reversal symmetry (in the absence of magnetic fields), for any given eigenfunction $\psi(\mathbf{r})$ with an expected momentum $\langle p_x\rangle$ there is another eigenstate (the complex conjugate of the former) associated with same energy and propagating with momentum $-\langle p_x\rangle$. As a consequence, all eigenstates can be taken to be real (and are taken to be so in the Lanczos algorithm employed in the following), as shown by the transformation $\psi_1=(\psi$

$+\psi^*)/\sqrt{2}$, $\psi_2=(\psi-\psi^*)/\sqrt{2}i$. In this case the expected momentum of all eigenstates will be zero, *even if* the states represent delocalized states. The momentum module of the original eigenfunctions can be recovered by calculating the matrix element $\langle\psi_1|p_x|\psi_2\rangle$, which is the quantity appearing in Eq. (1). In practice, it is known that in a finite disordered system the probability that an energy level is degenerate is zero, being only strictly degenerate in the infinite system.[32] However, the minimum energy distance between two extended levels goes to zero as the size of system is increased, and in fact, the matrix element considered in Eq. (1) is the relevant quantity determining the zero-frequency conductivity as expressed by the Kubo equation [Eq. (4)].

Resta and Sorella[28] have proposed a localization definition that avoids any reference to the excitation spectrum. They showed that the dimensionless complex number $z=\langle\psi|e^{i(2\pi/L)x}\psi\rangle$ tends to one when the state is localized and to zero when it is delocalized in the limit $L\to\infty$. This definition is not restricted to a one-electron representation, they also showed that the trivial extension of the formula to a many-body system still tends to one for insulating systems (either independent electrons or correlated, either crystalline or disordered) and to zero for metals. We have tried to apply this criterion to our data. However, the results are not conclusive, as the method requires the size of the system to be much bigger than the typical localization length λ. In that case it can be expanded as $z\sim1-(2\pi/L)^2\lambda^2/2$. If, for example, the size of the system is only six times the localization length, then the first correction would be 0.55, and z still far from unity. In contrast, the localization method we propose depends only on the value of the wave functions at the boundaries and will be valid provided the cell contains the localized wave function.

The approach we have outlined in this section for deciding if states of a finite periodic system are localized or extended can be applied once we have evidence that the properties of the states of this small system are representative of the infinite system we are trying to study. The approach we employ here for this purpose involves comparing the transport properties of finite systems of different size as detailed in Sec. IV.

B. Kubo–Greenwood equation

The electrical conductivity in the low field limit is given by the Kubo–Greenwood formula,[33] which in the independent electrons approximation can be written as[34]

$$\sigma=-\int dE\,\sigma(E)\frac{\partial f}{\partial E}, \tag{3}$$

where $f(E)$ is the Fermi distribution and $\sigma(E)$ is the conductivity at zero temperature,

$$\sigma(E)=\frac{2\pi e^2\hbar\Omega}{m^2}|(p_x)_{\alpha\beta}|^2_{\mathrm{av}}g(E)^2, \tag{4}$$

where Ω is volume of the system and $g(E)$ is the density of states per unit energy in each spin direction, per unit volume. The suffix ''av'' denotes an average over all states having energy within an interval Δ around E:

$$|(p_x)_{\alpha\beta}|^2_{\mathrm{av}}=\frac{1}{N_\Delta^2}\sum_{\alpha,\beta}|\langle\alpha|p_x|\beta\rangle|^2, \tag{5}$$

where N_Δ is the number of states inside that energy interval. This expression together with $g(E)$ must be averaged over all the configurations of the atoms (considered as classical particles) in the ensemble. The conductivity is obtained in the double limit $\Omega\to\infty$ and $\Delta\to0$, which should be carried out simultaneously.[28]

If the states from a range of energies are localized, the expected momentum vanishes and Eq. (4) predicts no contribution to the conductivity. There can still be conduction due to hopping assisted by phonons, a mechanism not included in this version of the Kubo equation, but usually it involves mobilities orders of magnitude smaller than the contribution due to extended states. In our case the concentration of excess electrons is very low, and thus the electron gas is nondegenerate and the Fermi distribution becomes Maxwellian. Therefore, we can write the mobility $\mu=\sigma/en$ (n being the excess electron number density) as

$$\mu=\frac{\pi e\hbar^3\Omega\beta}{m^2}\frac{\int dE\,K(\Omega,E)^2g(E)^2e^{-\beta E}}{\int dE\,g(E)e^{-\beta E}}, \tag{6}$$

where $\beta\equiv1/k_BT$ and

$$K^2\equiv|(p_x)_{\alpha\beta}|^2_{\mathrm{av}}/\hbar^2. \tag{7}$$

We shall see that even at room temperature k_BT (0.026 eV) is small compared to the typical energy range of $g(E)$ ($\sim$0.1 eV). Consequently, the main contributions to the integrals in the numerator and denominator in Eq. (6) come from a small interval around E_c (the mobility edge E_c separates localized and extended states) and the region close to the minimum energy E_0, respectively.

In a perfect lattice, with a given fixed density of scatterers, K^2 is a function of energy alone, and Eq. (6) gives the expected divergence when the system volume is taken to infinity. In order to obtain a finite mobility, K^2 must decay as Ω^{-1} when $\Omega\to\infty$. This can be understood by means of simple considerations due to Mott.[34] Assuming that the phases of the wave function in two different regions are uncorrelated if they are separated by a distance bigger than λ, the coherence length (also called mean free path), the integral K can be expanded as a sum over different regions Γ_j of volume λ^3:

$$K=\sum_j K_j,$$

where

$$K_j=\int_{\Gamma_j}d\mathbf{r}\,\psi(\mathbf{r})^*\frac{1}{i}\frac{\partial}{\partial x}\psi(\mathbf{r}). \tag{8}$$

Since the phases are uncorrelated in different regions the variables K_j will be uncorrelated, leading to $K^2=\Sigma_jK_j^2=(\Omega/\lambda^3)K_j^2$, where Ω/λ^3 is the number of such regions. For extended states the wave function can be written as $\psi(\mathbf{r})=\phi(\mathbf{r})/\sqrt{\Omega}$, where $\phi(\mathbf{r})$ is a complex function with a modulus of the order of the unity. In the quasifree particle picture $\phi(\mathbf{r})\approx\exp(i\mathbf{k}\cdot\mathbf{r})$, where $\mathbf{k}$ is a vector of magnitude

$k=\sqrt{2mE}/\hbar$ and a random direction in each region Γ_j. With these approximations it is easily shown that the correct behavior in the limit $\Omega\to\infty$ is satisfied:

$$K^2 \sim \frac{1}{\Omega}\frac{\left[\int_{\Gamma_j} d\mathbf{r}\,\phi(\mathbf{r})^* \frac{1}{i}\frac{\partial}{\partial x}\phi(\mathbf{r})\right]^2}{\lambda^3}. \tag{9}$$

Note that if the size of the system is smaller than the typical coherence length λ the integral in Eq. (9), and thus the computed mobility, will give a value smaller than the actual mobility in the real (larger) system.

C. Simulation details

We have used the molecular dynamics code DLPOLY[35] to generate molecular configurations at finite temperature. We have modeled the *n*-alkane fluids using a united atom model.[36] The force field includes bonded (bond stretch,[37] valence angles, and dihedrals[38]) and dispersion interactions. In contrast the amorphous regions of PE at $T=300$ K were modeled using an *all-atom* force field described in Ref. 39 employing a single chain in a periodic simulation cell. Various PE system sizes were used (at constant density) ranging from 87 to 2880 CH_2 units (of three atoms). The following procedure was employed: an initial low density configuration of the chain was generated using a Monte Carlo algorithm, then the system was compressed in a constant pressure molecular dynamics run until the density reached the experimental value[40] of amorphous PE ($\rho=0.855$ g cm^{-3}) at room temperature. Finally, the system was brought to a local equilibrium in the microcanonical ensemble. The pair correlation functions, dihedral angle distribution, and thermodynamic properties were independent of the procedure used to prepare the system. We obtained good agreement with a system obtained by quenching, previous simulations,[41] and experimental data.[42] Note that at 300 K simulated and experimental amorphous states of PE are above the glass transition.[42]

A fast Fourier transform block Lanczos diagonalization algorithm[31,43] was used to compute the adiabatic excess electronic states of the static configurations taken from the molecular simulation. This method provides the lowest energy eigenstates for a given three-dimensional potential energy grid, and has been used successfully to describe excess electrons in simple fluids.[44] We used a fixed grid spacing of 0.7 Å, though for the large fluid systems we used 1 Å. We have tested the convergence of our calculations with grids of smaller spacing. As an example, in amorphous PE, using grids of 22^3, 32^3, and 64^3 points (corresponding to uniform grid spacings of 0.97, 0.67, and 0.33 Å) we obtained a ground-state energy of $E_0=-0.134\,55$, $-0.107\,91$, and $-0.107\,55$ eV, respectively, which implies an energy resolution of 0.03 eV.

The polarization interaction between the electron and the induced dipoles in the system was computed self-consistently using an iterative algorithm (see Sec. III). The electron–atom interactions were truncated at $r_c=9$ Å. All reported electronic energies include a long-range correction V_c based on a perturbation theory partition of the pseudopotential for disordered systems: $V_c=-2\pi\alpha n a_L/r_c$,[44] where α is the isotropic polarizability of the molecules or (united) atoms, n the corresponding number density, and $a_L=[1+(8/3)\pi n\alpha]^{-1}$ the Lorentz local-field factor. For highly ordered systems the long-range correction can be computed using the form $V_c=-A/r_c$, where A is a constant obtained by linear fitting the data at different cutoffs. As a test of the isotropic correction, using the ground-state energies for amorphous PE with $r_c=9$ and 12 Å we obtained $A=3.89$ Å eV, which leads to a long-range correction consistent with the isotropic correction data within a margin of 0.007 eV.

III. PSEUDOPOTENTIALS

The potential energy between an excess electron at $\mathbf{r}$ and a system of (united) atoms at $\mathbf{R}_i$ can be written as

$$V(\mathbf{r},\mathbf{R}_i)=\sum_j V_j^r(|\mathbf{r}-\mathbf{R}_j|)+V^p(\mathbf{r},\mathbf{R}_i), \tag{10}$$

where $V_j^r(r)$ is a short-range repulsive pair potential which accounts for the interaction with the static charge distribution as well as exchange and orthogonality of the excess electron with the target atom. The second term represents the charge-induced-dipole polarization interaction:

$$V^p(\mathbf{r},\mathbf{R}_i)=-\frac{1}{2}\sum_j \mathbf{p}_j\cdot\mathbf{E}_j^{(0)} S_j(|\mathbf{r}-\mathbf{R}_j|), \tag{11}$$

where

$$\mathbf{E}_j^{(0)}=-e\frac{\mathbf{R}_j-\mathbf{r}}{|\mathbf{R}_j-\mathbf{r}|^3} \tag{12}$$

is the direct electric field due to the excess electron,

$$\mathbf{p}_j=\alpha_j\mathbf{E}_j \tag{13}$$

the dipole moment of the atom j, α_j the corresponding polarizability tensor, and $S_j(r)$ is a switching function which describes the screening of the electric field due to the charge distribution of the atom as the electron approaches it. This function goes to 1 as the electron separates from the target atom. In Eq. (13) $\mathbf{E}_j$ is the local electric field at the atom j, which is the superposition of the Coulomb field of the excess electron and the electric fields due to all the other induced dipoles

$$\mathbf{E}_j=\mathbf{E}_j^{(0)}+\sum_{k\neq j} T_{jk}\cdot\alpha_k\mathbf{E}_k, \tag{14}$$

with $T_{jk}=(3\hat{\mathbf{r}}_{jk}\hat{\mathbf{r}}_{jk}-1)/r_{jk}^3$. The set of equations (14) can be solved self-consistently using an iterative approach. However, if the atoms or molecules in our system are isotropic and the macroscopic state is disordered, then we can use a much less expensive mean-field approach,[44,45] where the local field is approximated by $a(r)\mathbf{E}_j^{(0)}$. Here $a(r)$ is a mean-field screening function solution of an integral equation that is a function of the density and the pair correlation function of the system.[45] In general this function decays from unity to the Lorentz local factor a_L in an oscillatory fashion. With this approximation the potential energy becomes pairwise additive, with a polarization contribution $V_p(r)=-\alpha e^2 S(r)a(r)/2r^4$.

TABLE I. Pseudopotential parameters. Energies in electron volts and lengths in angstroms.

	B_1	B_2	δ
CH_4	3.97	3.53	
CH_3	3.97	3.53	0.3
CH_2	4.41	3.92	0.44

A. *e*-CH_4 pseudopotential

We have utilized the pseudopotential used in Ref. 46 to describe the interaction between an excess electron and a molecule of methane. It involves a repulsive component $V_r(r)=\Sigma_{i=1}^{2} A_i \exp(-B_i r)$, with $A_1=8160$ eV and $A_2=-3590$ eV, combined with the switching function $S(r)=(1-e^{-r/r_0})^6$ with $r_0=0.622$ Å. The parameters in the repulsive term are summarized in Table I. These parameters were adjusted to give agreement with $l=0$ phase shift data obtained from *ab initio* calculations.

Methane is a spherical molecule, with a polarizability of $\alpha=2.6$ Å^3.[47] In an isotropic fluid of spherical particles mean field theory should be reliable. Figure 1 compares the ground state energies obtained with the mean-field approximation with the values from a full many-body polarization calculation and experimental results for various methane densities at $T=340$ K. The data comprise averages over 10 different configurations of 512 methane molecules. Both computed curves agree well with the experimental values of V_0. Simulations at $T=180$ K resulted in consistent data.

B. *e*-CH_3 and *e*-CH_2 pseudopotentials

In order to obtain a pseudopotential transferable to other alkanes we have considered the higher alkanes, ethane and propane. The electron–methane pseudopotential cannot be used directly to describe the interaction with ethane because of the anisotropy of the molecule.[46] This anisotropy is manifested in both repulsive and attractive (polarization) parts of the pseudopotential. The polarizability tensor in ethane is anisotropic; the component along the axis of the molecule is larger than that in the perpendicular directions.[47] In Ref. 46 this anisotropy was accounted for by placing an exponential repulsive center in the middle of the C–C bond. Although modeling a long-range interaction ($\sim r^{-4}$) anisotropy with a short-range term (exponential) is not optimal, it can be adjusted to force agreement with the experimental data in the fluid density range. However, when used in high density systems as polyethylene we have found that it leads to an underestimation of the conduction band level by several electron volts. Instead we have used the multicenter polarizabilities given in Ref. 48, which were obtained using *ab initio* calculations. In this approach the electrostatic potential created by the alkane molecule due to the presence of the electron is reproduced by a distribution of dipoles located at the hydrogen and carbons atoms, as well as at the center of the C–C bond. Using this set of polarizabilities we obtain the following polarizability tensors (in Å^3) for the methyl and methylene groups:

$$\alpha_{CH_3}=\begin{pmatrix} 1.27 & & \\ & 2.04 & \\ & & 2.04 \end{pmatrix}, \tag{15}$$

and

$$\alpha_{CH_2}=\begin{pmatrix} 0.5 & & \\ & 1.12 & \\ & & 1.64 \end{pmatrix}. \tag{16}$$

In Eq. (15), the x axis is defined along the C–C bond, whereas in Eq. (16) the x axis should be taken in the direction defined by the two nearest carbon neighbors in the molecule and the y axis inside the plane of the carbon nuclei (see Fig. 2). The set of polarizabilities is completed with the polarizability tensor of the bond C–C, which is represented as a

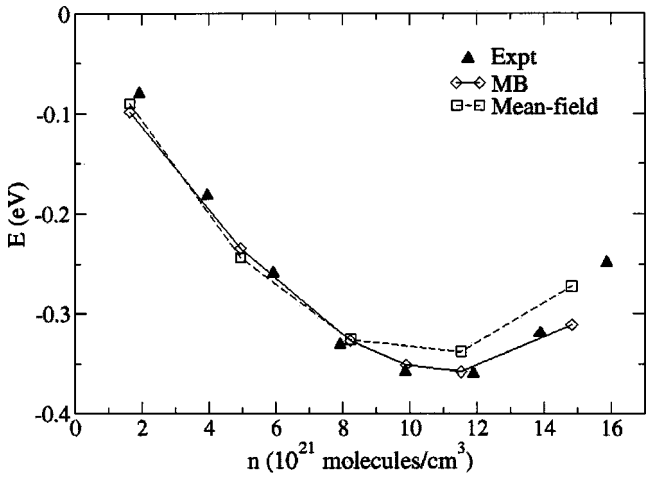

FIG. 1. Excess electron ground state energies in methane. Closed triangles are the experimental V_0 values (Ref. 58), diamonds the full many-body polarization, and squares the mean-field results.

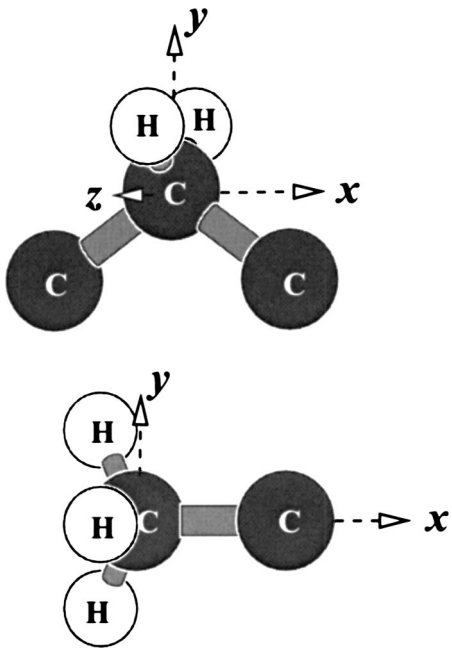

FIG. 2. Scheme showing the axes defined in the text for the CH_2 and CH_3 units.

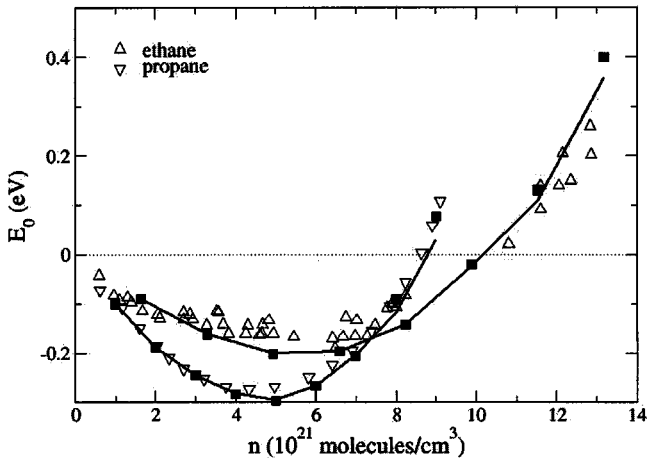

FIG. 3. Excess electron energies in ethane and propane. Computed ground state values (lines), mobility edge (closed squares), and experimental V_0 (triangles) as a function of the number molecular density.

new site centered at the middle of the C–C bond with a component $\alpha_{C-C}=2.103$ Å^3 in the bond direction, and zero in the perpendicular directions. Because these polarizabilities were calculated neglecting the intramolecular dipole–dipole interaction (up to *n*-butane[48]), we did not compute the direct dipole–dipole interactions when the two centers were closer than a certain distance, taken as $r_{mbmin}=3$ Å. The results were insensitive to any reasonable choice of this parameter.

In Ref. 49 the excess electron wave function corresponding to the bottom of the conduction band of crystalline PE is calculated using density functional theory (DFT). It can be seen in Fig. 3 of Ref. 49 that the CH_2 units act as repulsive sites for the electron, displaced $\delta\sim0.4$ Å from the carbons atoms in the direction of the hydrogens. This study is based on the identification of the Kohn–Sham eigenstates with excited states, which is not a rigorous procedure, and it is known that it leads to energies that underestimate band gaps by several electron volts.[50,51] Nevertheless, the Kohn–Sham equations can be interpreted as a mean-field approximation for a single electron, and thus it may provide a qualitative description for electron states. Consequently, we have included this feature in our pseudopotential model (Table I lists the displacements δ from the centers of the carbon atoms). In the methyl group the displacement is away from the methyl along the C–C bond direction, whereas in the methylene groups it is along the *y* axis defined in Eq. (16) (see Fig. 2).

For the repulsive and switching functions in the pseudopotential we have used the same functional form as for methane, but readjusted the parameters in order to get good agreement with the experimental data for the ground state energies in ethane and propane. The parameters are listed in Table I.

Figure 3 shows the calculated ground-state values for ethane and propane at $T=340$ K and $T=426$ K, respectively, together with the experimental data taken from Refs. 52 and 53. The calculated values were averaged over 10 configurations of 216 alkane molecules (systems of 1728 molecules produced consistent data). As we shall see later on, the mobility edge in these systems lies close to the average ground-state energy, and hence to the experimental value of V_0.

In order to probe our pseudopotentials we have considered two different situations. In the first case the polarizability centers of the methyl methylene units are kept at the center of the carbon atoms, while the repulsive centers are displaced as discussed before. In the second case the polarizability centers are placed together with the repulsive centers. Both pseudopotentials produced energies in agreement with the experimental data and to each other within 0.07 eV, which we consider a good estimate of the accuracy of our pseudopotentials.

C. Surface effects

The energy origin in our pseudopotential is such that the interaction energy tends to zero when the electron separates from the atoms. Therefore, it is tempting to identify the zero of energy with the vacuum level. However, this pseudopotential does not take into account the distortions in the electrostatic charge distribution near the surfaces, which results in a net dipole moment creating a electrostatic potential drop.[54] Thus, the zero of energy is usually slightly below the vacuum level by a quantity W_s, which depends on the details of the surface itself. We have performed *ab initio* calculations of the crystal surfaces (001) and (110) to determine W_s using the density functional theory code CASTEP[55] within the CGA, Perdew–Burke–Ernzerhof gradient correction.[56] Following the method introduced by Baldereschi *et al.*,[57] we first computed the mean electrostatic step D_s across the slab surface using the total (electronic and nuclear) charge density obtained with the DFT code. The plane-averaged electrostatic potential $\overline{V}_{el}(z)$ (taking the *z* axis perpendicular to the surface) is then obtained by integrating the one-dimensional Poisson equation. We first considered the surface (110), for which the PE chains are arranged in infinite layers parallel to the surface. Inside the bulk these layers are separated from each other by a distance 4.105 Å. The slab contained 6 layers, with a vacuum thickness separating the slab of 17 Å. Both surfaces of the slab were kept equivalent, thereby avoiding dipole interactions between the surfaces. In addition we calculated the charge density of a simple layer in a supercell of 15 Å for which surface effects are absent. The electrostatic potential is obtained by simply adding the contribution of each layer. W_s can be estimated as the difference between the dipole strength D_s in each case giving $W_s=0.03\pm0.02$ eV. To study the dependence on the surface type we have also computed the charge density of a (001) PE slab, where the chains are perpendicular to the surface, using the chain fold proposed in Ref. 58. This gave $W_s=0.07\pm0.03$ eV, which implies an energy difference between the two surface types of 0.04 ± 0.03 eV, in reasonable agreement with the value of 0.07 eV reported in Ref 58. The large error bars come from the fact that we are measuring very tiny differences (about 1% of $D_s\sim5.5$ eV). In fact, these values are of questionable significance, as we do not expect DFT to be capable of such accuracy. Nevertheless, they imply that corrections due to surface effects are small and can be neglected. This result agrees with simple electrostatic consid-

TABLE II. Localization criterion data. Energies in electron volts and lengths in angstroms.

	L	E_1	E_2	$p_x/\hbar$	$\Phi_x/\hbar$
Methane	74.55	−0.343	−0.342	0.0195	0.0163
Ethane	53.11	0.102	0.124	0.0039	0.0002
		0.102	0.140	−0.0055	−0.0001
		0.124	0.140	−0.0088	−0.0001
		0.140	0.143	−0.0276	−0.0222
Amorphous PE	32.11	−0.017	0.008	−0.0054	0.0006
		0.055	0.059	0.0167	0.0145
		0.119	0.125	0.0176	0.0159

erations, which predict no correction at all as long as the molecules are not drastically truncated at the surfaces since alkanes are nonpolar molecules.

IV. RESULTS

A. Methane

Simple inspection of the excess electron wave function in fluid methane shows that the ground state is clearly extended throughout the whole density range shown in Fig. 1. The localization criterion presented in Sec. II cannot be applied to excess electron ground state wave functions because even though they are extended, e.g., being Bloch functions, they are usually at the bottom of the band and thus with a vanishing momentum. However, it can be applied to the excited states. Table II shows the x component of the expected momentum of the wave function $\psi=(\psi_1+i\psi_2)/\sqrt{2}$, where ψ_1 and ψ_2 are the first two excited levels, for a typical configuration of the fluid with number density 9.85×10^{21} cm^{-3}. This momentum can be readily evaluated using the fast Fourier transform algorithm, and is equivalent to the matrix element in Eq. (1) except for a phase factor. The minimum extended correction Φ_x is very close to the expected momentum, showing the extended nature of the spectrum. This result is consistent with the high mobility found in experiments.[59] In order to calculate the mobility we have computed the density of states for a methane fluid of density 9.85×10^{21} cm^{-3} at $T=180$ K. The histogram of the first 25 levels, averaged over 10 configurations, can be summarized as a density of states per spin (as shown in Fig. 4) which we have fit to the form $g(E)\approx11.9(E-E_0)$ eV$^{-1}\times10^{21}$ cm^{-3} in the energy interval $-0.36<E<-0.15$ eV, where $E_0=-0.36$ eV. The density of states was insensitive to temperature; we obtained the same results at $T=340$ K. Using the Kubo–Greenwood equation (6) we estimate $\mu\approx102$ cm^2/V s, which is small compared to the experimental value, $\mu\approx1000$ cm^2/V s. This discrepancy can be explained in terms of the deformation-potential theory,[21] which when used with the experimental V_0 values (as a function of the molecular density) provides the correct shape of the experimental mobility against the density and acceptable quantitative agreement far from the critical density in methane.[60] This semiphenomenological theory is based on the assumption of free-particle-like behavior, inferred from the high experimental value of the mobility, and can be seen as a consequence of the mobility edge lying at the bottom of the band

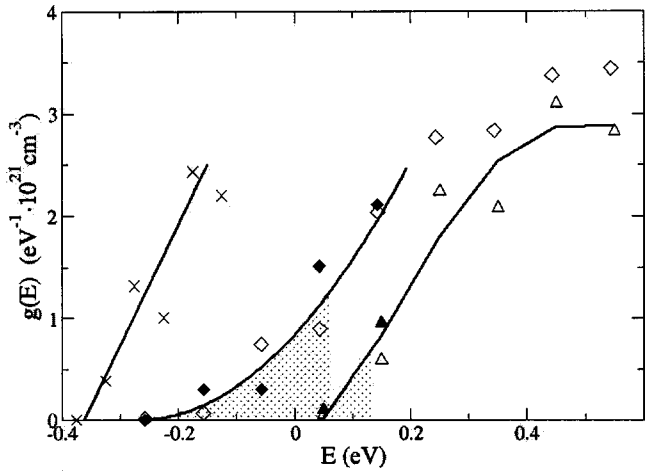

FIG. 4. Density of states per unit of volume, energy, and spin for methane with $\rho=9.85\times10^{21}$ cm^{-3} (crosses), amorphous PE (diamonds) at room temperature, and ethane with $\rho=11.53\times10^{21}$ cm^{-3} (triangles). Closed symbols are data from larger systems plotted to test consistency. The lines for methane and PE are the polynomial fits used in the text, whereas for ethane it is a guide to the eye.

($E_c\sim E_0$). Following Basak and Cohen,[21] at thermodynamic equilibrium only the lower levels will contribute to the conductivity. As a result, the corresponding eigenstates will have considerable amplitude Fourier components on the scale of the thermal de Broglie wave number, in addition to the large amplitude Fourier components on the much smaller scale of the inverse of the interatomic separation produced by the local disorder. This involves two different coherence lengths. The shorter length is responsible for the decay of the averaged square momentum matrix element K^2 [defined in Eq. (7)] as a function of the system volume in the length scale of the simulations, which is shown in Fig. 5. The data correspond to the bottom of the band of systems with sizes $L=23.30$, 37.28, 55.91, and 74.55 Å, and an average energy interval $\Delta=0.13$, 0.05, 0.02, and 0.01 eV, respectively. However, as shown in the inset of Fig. 5, the largest system size is not big enough to reach a plateau of ΩK^2 values, because the thermal coherence length is still larger. Assuming an effective mass of the order of unity for the excess electron, its

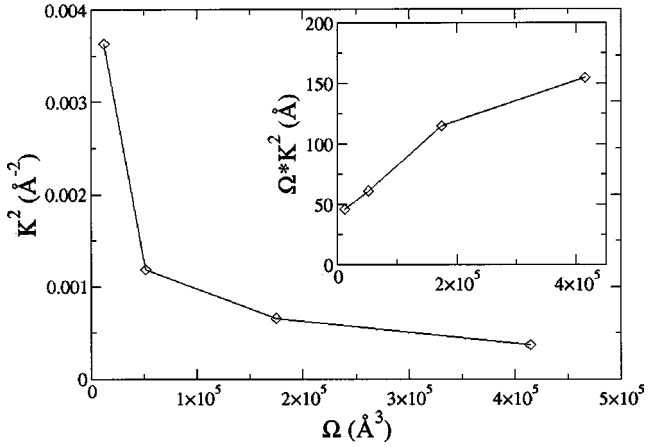

FIG. 5. Averaged momentum K^2 (7) at the mobility edge as a function of the system volume for methane.

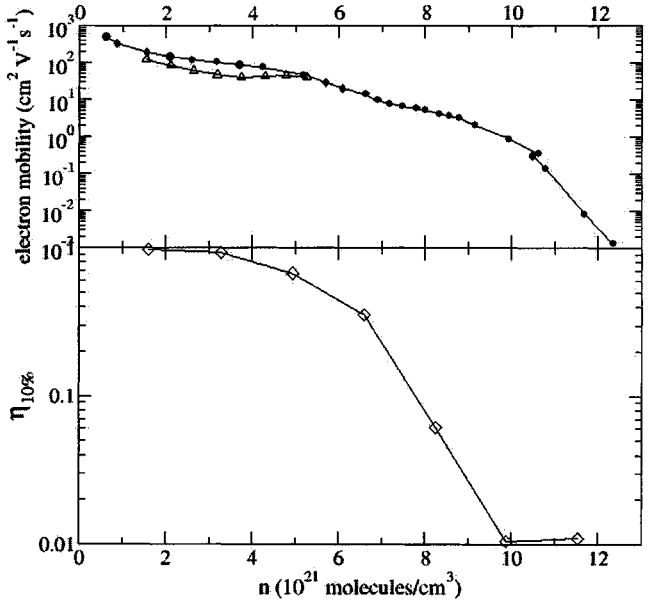

FIG. 6. Fraction of the volume occupied by the excess electron as a function of the fluid density for a fixed system length of $L=44.1$ Å. The upper plot shows the experimental electron mobility of ethane at $T=340$ K (closed circles) and $T=305.33$ K (open triangles)—Ref. 22.

thermal de Broglie wavelength will be of the order of 100 Å, bigger than the largest system simulated. The corresponding wave numbers are only scattered by the long-range fluctuations of the potential created by local density fluctuations. A proper calculation of the mobility in such a quasifree state would involve simulating systems of at least twice the linear dimension we have considered (i.e., 8 N). Because of the grid techniques we are using, that is beyond our present resources.

B. Ethane and propane

The ground-state energies for excess electrons in ethane shown in Fig. 3 are calculated from unperturbed configurations of the ethane molecules at 340 K. It is known that for high fluid densities the excess electron, in nonpolar and polar solvents,[61] may interact strongly with its environment, pushing the surrounding molecules aside and lowering its energy[46,62] by creating a bubble. This is also expected from the abrupt drop of the mobility in ethane at about $\rho\approx 10\times 10^{21}$ cm^{-3} (Ref. 22) (Fig. 6, top). The abrupt mobility drop can be explained by considering the fraction of the volume occupied by the localized electron as a function of the fluid density. Figure 6 shows the fraction η of volume where the excess electron ground state has a density probability larger than 10% of its maximum plotted over a range of unperturbed fluid ethane densities and for a fixed unit cell of $L=44.1$ Å. The electron, and thus its interaction with the solvent, is spread throughout much of the simulation box for low fluid densities and hence will not exert a large force on nearby molecules, but the electron becomes increasingly concentrated for the higher densities. For densities above 10×10^{21} cm^{-3} the excess electron is restricted to a small region of the box, where the concentrated quantum forces are able to create a bubble. This localization does not take place when the electronic states are computed using the CH_4 pseudopotential centers at the ethane carbon atoms instead of our proposed CH_3 pseudopotentials for the same configurations.[46] Therefore, it is a consequence of the reduced free volume seen by the electron because of the displacement δ of the CH_3 repulsive core from the ethane carbon atoms, which effectively breaks the paths where the excess electron can propagate if ethane is viewed as pairs of CH_4 centers.

The reduction of the wave function extension is a general property of the energy spectrum, but does not necessarily mean that all states are localized. Table II shows the localization criterion data for a typical unperturbed configuration of the fluid ethane with $\rho=11.53\times 10^{21}$ cm^{-3}. The comparison of the first excited level $E_1=0.102$ eV with the other levels indicates that it is localized, but levels above 0.140 eV show clear delocalization, even though the corresponding fraction of the volume occupied in this excited state is as low as $\eta=0.03$. We have repeated this analysis for 10 different configurations, and obtained the average mobility edge $E_c=0.13$ eV, as shown in Figs. 3 and 4. We also present in Fig. 4 the corresponding density of states for this fluid ethane state point, calculated averaging over 10 configurations of a system of 216 (open triangles) and 1728 (closed triangles) ethane molecules. A similar calculation for the highest density considered, $\rho=13.18\times 10^{21}$ cm^{-3} in a simulation box of length $L=50.8$ Å, leads to a mobility edge located at 0.40 eV, and then only 0.05 eV above the averaged ground state level. Thus we see in these unperturbed fluid ethane configurations that as the density is increased the gap between localized states at low energy and delocalized states at higher energies narrows to about k_BT at the highest fluid densities considered in these studies.

We have computed the mobility edge as a function of density for a system of 1728 molecules of propane following the same procedure as for ethane. The results are shown in Fig. 3, which shows a transition to localized states at about $\rho=7.5\times 10^{21}$ cm^{-3}.

C. Amorphous PE

The number density of carbon atoms is typically about 1.5 times that of the densest fluid alkanes discussed in the previous sections. Due to the high molecular density of amorphous PE, the lowest states are always localized in the regions where the density is lowest (since PE is a solid we do not expect the electron to significantly alter the local density unlike for high density liquids). The minimum energy electronic state obtained in the simulations is located below the vacuum level at -0.32 eV. This is in good agreement with experiments on molten long-chain alkanes, where the ground state energy was also found to be negative.[63] Analysis of the function $K^2(E,\Omega)$ as well as the localization criterion data locate the mobility edge E_c at about the zero energy level. This is confirmed in the two largest systems considered, i.e., systems containing 1215 and 2880 CH_2 units provided the values $+0.055$ eV (see Table II) and $+0.072$ eV, respectively. Figure 7 shows the ground state wave function and a typical extended state above the mobility edge for a given

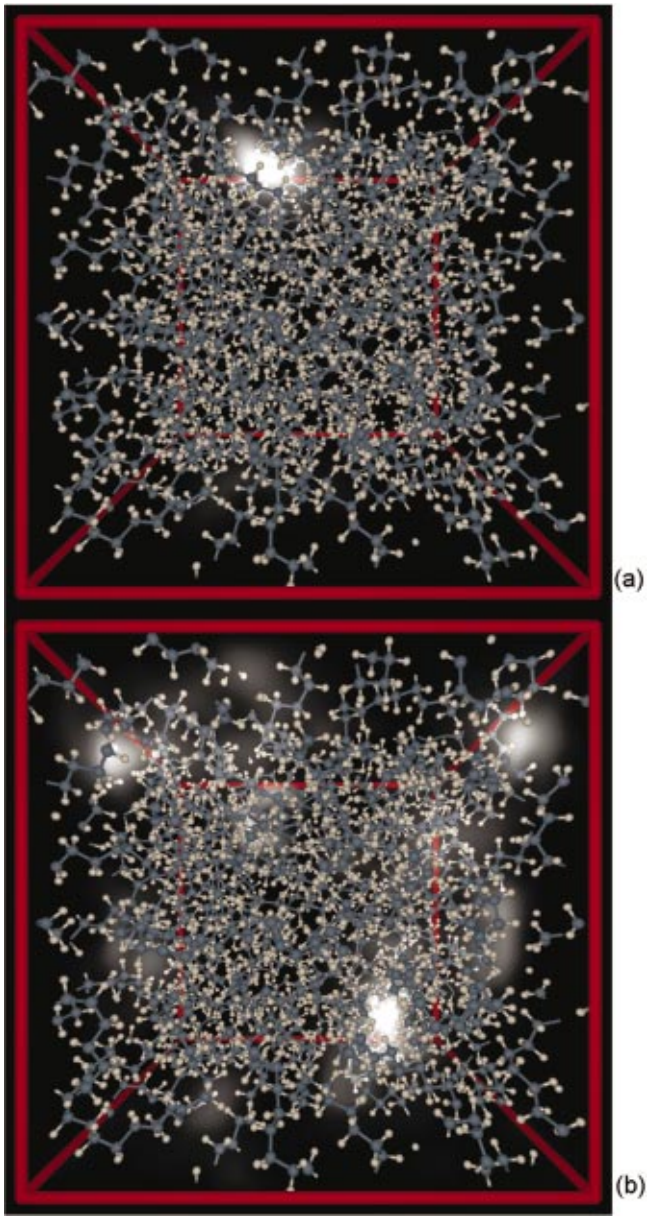

FIG. 7. (Color) Volumetric representation of the excess electron density probability for a typical configuration of amorphous PE at room temperature. (a) Ground state corresponding to $E_0=-0.12$ eV showing localization. (b) Typical extended state, with energy 0.12 eV. The lighter the region, the bigger the density probability.

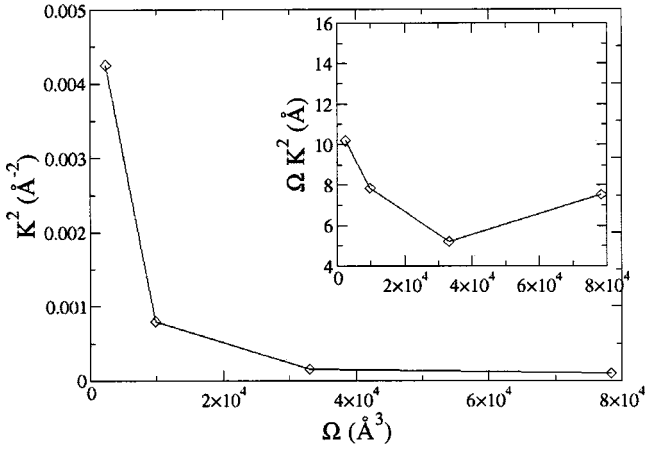

FIG. 8. Averaged momentum K^2 (7) at the mobility edge as a function of the system volume for amorphous PE at room temperature.

configuration of the material at room temperature and a system size of 32.12 Å. The ground state is completely localized in a region of about 7 Å, whereas in the extended state the wave function is spread through the entire simulation cell.

We have computed the density of states of amorphous PE (averaging over 75 configurations) modeled with a single chain of 360 CH_2 units. The data can be fitted in the energy interval $-0.27<E<0.2$ eV to the expression $g(E)\approx 11.6(E-E_0)^2$ eV$^{-1}\times 10^{21}$ cm^{-3}, where $E_0=-0.27$ eV, as shown in Fig. 4. A larger system of 1215 CH_2 units produced consistent data (closed diamonds in Fig. 4). In Fig. 8 we present the calculated values of K^2 at the mobility edge for fixed density PE samples ($\rho=36.7\times 10^{21}$ CH_2 units per cm^3) with lengths $L=13.38$, 21.41, 32.12, and 42.80 Å, and an average energy interval $\Delta=0.13$, 0.05, 0.02, and 0.01 eV, respectively. The inset shows convergence, indicating that the longest coherence length of the excess electron is smaller than the size of the systems considered. As a consequence we are able to compute the electron mobility. In this case $E_c-E_0\gg k_BT$, and thus Eq. (6) can be written as an activated mobility $\mu=\mu_0\exp(-(E_c-E_0)/k_BT)$, with an activation energy of $E_c-E_0\approx 0.33$ eV. This value is in good agreement with the apparent trap depth of 0.35 eV estimated from thermally stimulated conductivity and thermoluminescence measurements[64,65] as well as activation energies estimated from electron-beam-induced conduction[66] or the value 0.24 eV given by Tanaka and Calderwood,[67] which have already been attributed to the amorphous part of PE. Using our data we then obtain a prefactor $\mu_0\approx 750$ cm^2/V s and an excess electron mobility of $\mu\approx 2\times 10^{-3}$ cm^2/V s. Note that the present energy resolution produces an uncertainty in the mobility of about one order of magnitude (due to the exponential factor). This value compares favorably with the reported values in PE, which is in the range 10^{-3}–10^{-10} cm^2/V s.[68] It has been suggested[69] that the striking range of variation of the mobility values reported by various investigators is mainly due to the different measurement procedures adopted, and in particular to the measurement time for each particular experiment. When the conduction takes place over very long times, carrier trapping and therefore space charge formation become dominant, providing the lowest values of the apparent mobility.

V. CONCLUSIONS

In this paper, we have presented a semiempirical pseudopotential derived to be consistent with experimental data for the density dependence of the threshold of conduction in fluid ethane and methane. The pseudopotential consists of a repulsive component constructed from *ab initio* calculations in methane and crystalline PE and an anisotropic attractive part which accounts for the polarization interaction between the excess electron and the dielectric. The electronic states obtained with this pseudopotential are in good agreement with the experimental data in alkane fluids and polyethylene.

We have also introduced a new localization criterion that successfully predicts the nature of the electronic states in methane and ethane. When applied to fluid propane it leads us to predict a transition between an extended ground state and a localized ground state at the molecular density $\rho = 7.5\times10^{21}$ cm^{-3}. In amorphous PE at room temperature it has allowed us to locate the mobility edge at about the vacuum level. This implies a trap depth energy of about 0.3 eV due to local disorder, in good agreement with the experimental data.[64–67] The location of the mobility edge should be compared with the conduction band level of $+0.6$ eV found in crystalline PE.[23] In materials with low degrees of crystallinity this energy difference would prevent the electron from penetrating the crystalline regions and conduction would only occur through the disordered regions.

We have been unable to compute the excess electron mobility in methane using the Kubo–Greenwood equation due to the limited system sizes employed in the simulation. However the electronic coherence length is much smaller in amorphous PE, allowing us to estimate the mobility at room temperature as $\mu \approx 2\times10^{-3}$ cm^2/V s. This value is at the upper limit of the range found in experimental estimates of real PE, i.e., with coexisting crystalline and amorphous regions. It is consistent with the behavior reported by Kosaki *et al.*,[70] where an abrupt increase of the mobility is observed when semicrystalline PE is heated beyond its melting point. Furthermore, since we have ignored in this study other important traps such as chemical traps[71] or those found at amorphous/crystalline boundaries, it is to be expected that our mobility would be higher than the values normally found experimentally. In particular, it is one order of magnitude larger than the mobility obtained by Tanaka and Calderwood using a ''run time'' method that minimizes the process of carrier capture and hence predicts high mobilities.[72]

Our calculations suggest an important new mechanism for excess electron transport in polyethylene: conduction through the excited states above the mobility edge in the amorphous regions. Our results depend upon neglecting the local conformational changes due to the presence of these excess electrons. To support this assumption we note that the characterization of the extended states using unperturbed configurations can be expected to be a good approximation since the perturbation of the environment by the electron is very small when it is delocalized. In addition, preliminary calculations of the nonadiabatic trajectories in these systems[73] show that after a time the electron self-traps with an energy corresponding to the bottom of the band in Fig. 4. The energy change due to the electron distorting the environment in this process is estimated to be small, $\sim$0.1 eV, of the order of the error bars in the present calculations, and therefore, the activation energy for excitation to extended states should be about 0.3 eV, which is close to the experimental findings.

ACKNOWLEDGMENTS

This work was supported by EPSRC through Grants No. GR/R18222 and No. GR/M94427. D.F.C. acknowledges support through a Schlumberger visiting Professorship of Chemistry at the University of Cambridge. D.F.C. also acknowledges support from NSF Grant No. CHE-9978320.

[1] The first polyethylene insulated cable was a mile of submarine cable between the Isle of Wight and the mainland of England installed by Dean's company in 1938, see J. A. Allen. *Studies in Innovation in the Steel and Chemical Industries* (Manchester University Press, Manchester, 1967).
[2] N. H. Ahmed and N. N. Srivinas, IEEE Trans. Electr. Insul. **4**, 644 (1997).
[3] A. Toureille, Rev. Gen. Electr. **8**, 15 (1991).
[4] Y. Li, T. Takada, and N. Takasu, J. Phys. D **26**, 986 (1993).
[5] R. E. Collins, J. Appl. Phys. **51**, 2973 (1980).
[6] J. Lewiner, IEEE Trans. Electr. Insul. **21**, 351 (1986).
[7] A. Dias Tavares, J. Chem. Phys. **59**, 2154 (1973).
[8] C. Le Gressus, F. Valin, M. Henriot, M. Gautier, J-P. Duraud, T. S. Sudarshan, R. G. Bommakandi, and G. Blaise, J. Appl. Phys. **69**, 6325 (1991).
[9] L. A. Dissado and J. C. Fothergill, *Electrical Degradation and Breakdown in Polymers* (Peregrinus, London, 1992).
[10] G. Blaise, J. Appl. Phys. **77**, 2916 (1995).
[11] L. A. Dissado, G. Mazzanti, and G. C. Montanari, IEEE Trans. Dielectr. Electr. Insul. **2**, 1147 (1995); **4**, 496 (1997); see also G. Mazzanti, G. C. Montanari, and L. Dissado, Proceedings of JICABLE'99, 1999, p. 707.
[12] M. Meunier and N. Quirke, J. Chem. Phys. **113**, 369 (2000); M. Meunier, A. Aslanides, and N. Quirke, *ibid.* **115**, 2876 (2001).
[13] G. Teyssedre, C. Laurent, A. Aslanides, N. Quirke, L. A. Dissado, A. Campus, and L. Martinotto, IEEE Trans. Dielectr. Electr. Insul. **8**, 744 (2001).
[14] J. A. Anta, G. Marcelli, M. Meunier, and N. Quirke, J. Appl. Phys. **92**, 1002 (2002).
[15] U. Asaf, R. Reininger, and I. Steinberger, Chem. Phys. Lett. **100**, 363 (1983).
[16] W. Döldissen and W. F. Schmidt, J. Phys. Chem. **84**, 1179 (1980).
[17] A. Krasinsky, U. Asaf, I. T. Steinberger, and R. Reininger, Chem. Phys. Lett. **231**, 536 (1994).
[18] M. G. Robinson and G. R. Freeman, Can. J. Chem. **52**, 440 (1974).
[19] K. Itoh, K. Nakagawa, and M. Nishikawa, J. Chem. Phys. **84**, 391 (1986).
[20] K. Nakagawa, K. Itoh, and M. Nishikawa, IEEE Trans. Electr. Insul. **23**, 509 (1988).
[21] S. Basak and M. H. Cohen, Phys. Rev. B **20**, 3404 (1979).
[22] W. Döldissen and W. F. Schmidt, J. Phys. Chem. **84**, 1179 (1980).
[23] D. Cubero, N. Quirke, and D. Coker, Chem. Phys. Lett. **370**, 21 (2003).
[24] D. Cubero, G. Marcelli, and N. Quirke, CIEDP, 2002.
[25] D. Cubero, N. Quirke, and D. Coker, Chem. Phys Lett. **370**, 21 (2003).
[26] R. Resta, J. Phys.: Condens. Matter **14**, R625 (2002).
[27] D. J. Thouless, J. Non-Cryst. Solids **8–10**, 461 (1972).
[28] P. A. Lee and T. V. Ramakrishnan, Rev. Mod. Phys. **57**, 287 (1985).
[29] R. Resta and S. Sorella, Phys. Rev. Lett. **82**, 370 (1999).
[30] J. T. Edwards and D. J. Thouless, J. Phys. C **5**, 807 (1972).
[31] M. H. Gutknecht, *Acta Numerica* (Cambridge University Press, Cambridge, 1997).
[32] K. B. Efetov, Adv. Phys. **32**, 53 (1983).
[33] G. D. Mahan, *Many-Particle Physics* (Plenum, New York, 1990).
[34] N. F. Mott and E. A. Davis, *Electronic Processes in Non-Crystalline Materials* (Clarendon, Oxford, 1979).
[35] W. Smith, C. W. Yang, and P. M. Rodger, Mol. Simul. **28**, 385 (2002).
[36] B. Smit, S. Karaborni, and J. I. Siepmann, J. Chem. Phys. **102**, 2126 (1995).
[37] Y. Jin and R. H. Boyd, J. Chem. Phys. **108**, 9912 (1998).
[38] W. L. Jorgensen, J. D. Madura, and C. J. Swenson, J. Am. Chem. Soc. **106**, 6638 (1984).
[39] R. Martonak, W. Paul, and K. Binder, Phys. Rev. E **57**, 2425 (1998).
[40] J. Brandrup and E. H. Immergut, *Polymer Handbook* (American Institute of Physics, New York, 1989).
[41] R. J. Roe, J. Chem. Phys. **100**, 1610 (1994).
[42] A. Koyama, T. Yamamoto, K. Fukao, and Y. Miyamoto, J. Chem. Phys. **115**, 560 (2001).
[43] F. Webster, P. J. Rossky, and R. A. Friesner, Comput. Phys. Commun. **63**, 492 (1991).
[44] B. Space, D. F. Coker, Z. H. Lui, B. J. Berne, and G. Martyna, J. Chem. Phys. **97**, 2002 (1992).
[45] J. Lekner, Phys. Rev. **158**, 130 (1967).
[46] Z. Liu and B. J. Berne, J. Chem. Phys. **99**, 9054 (1993).
[47] J. O. Hirschfelder, C. F. Curtiss, and R. B. Bird, *Molecular Theory of Gases and Liquids* (Wiley, New York, 1954).
[48] S. Nakagawa, Chem. Phys. Lett. **278**, 272 (1997).

[49] S. Serra, E. Tosatti, and S. Iarlori, Phys. Rev. B **62**, 4389 (2000).
[50] K. J. Less and E. G. Wilson, J. Phys. C **6**, 3110 (1973).
[51] B. Montanari and R. O. Jones, Chem. Phys. Lett. **272**, 347 (1997).
[52] Y. Yamaguchi, T. Nakajima, and M. Nishikawa, J. Chem. Phys. **71**, 550 (1979).
[53] K. Nakagawa, K. Ohtake, and M. Nishikawa, J. Electrost. **12**, 157 (1982).
[54] N. W. Ashcroft and N. D. Mermin, *Solid State Physics* (Saunders, Fort Worth, 1976).
[55] CASTEP 4.2 academic version, licensed under the UKCP-MSI Agreement, 1999; Rev. Mod. Phys. **64**, 1045 (1992).
[56] J. Perdew, K. Burke, and M. Ernzerhof, Phys. Rev. Lett. **77**, 3865 (1996).
[57] C. J. Fall, N. Binggeli, and A. Baldereschi, J. Phys.: Condens. Matter **11**, 2689 (1999).
[58] M. C. Righi, S. Scandolo, S. Serra, S. Iarlori, E. Tosatti, and G. Santoro, Phys. Rev. Lett. **87**, 076802 (2001).
[59] N. Gee and G. R. Freeman, Phys. Rev. A **20**, 1152 (1979).
[60] U. Asaf, R. Reininger, and I. Steinberger, Chem. Phys. Lett. **100**, 363 (1983).
[61] B. E. Springett, J. Jortner, and M. H. Cohen, J. Chem. Phys. **48**, 2720 (1968).
[62] T. Kimura and K. Fueki, J. Chem. Phys. **66**, 366 (1977).
[63] N. Ueno, K. Sugita, K. Seki, and H. Inokuchi, Phys. Rev. B **34**, 6386 (1986).
[64] T. Nishitani, K. Yoshino, and Y. Inuishi, Jpn. J. Appl. Phys. **14**, 721 (1975).
[65] T. Nishitani, K. Yoshino, and Y. Inuishi, Trans. Inst. Electr. Eng. Jpn., Part A **96-A**, 381 (1976).
[66] K. Yoshino, J. Kyokane, T. Nishitani, and Y. Inuishi, J. Appl. Phys. **49**, 4849 (1978).
[67] T. Tanaka and J. H. Calderwood, J. Phys. D **7**, 1295 (1974).
[68] M. Ieda, IEEE Trans. Electr. Insul. **EI-19**, 162 (1984).
[69] T. Tanaka, IEEE Trans. Dielectr. Electr. Insul. **8**, 733 (2002).
[70] M. Kosaki, M. Yoda, and M. Ieda, J. Phys. Soc. Jpn. **31**, 1598 (1971).
[71] M. Meunier, A. Aslanides, and N. Quirke, J. Chem. Phys. **115**, 2876 (2001).
[72] T. Tanaka and J. H. Calderwood, Trans. Inst. Electr. Eng. Jpn., Part A **93-A**, 473 (1973).
[73] D. Cubero, N. Quirke, and D. F. Coker (unpublished).